THE JOURNAL OF PHYSICAL CHEMISTRY B

Article

pubs.acs.org/JPCB

Destabilization of Alzheimer's Aβ42 Protofibrils with a Novel Drug Candidate wgx-50 by Molecular Dynamics Simulations

Huai-Meng Fan,[†] Ruo-Xu Gu,[†] Yan-Jing Wang,[†] Yun-Long Pi,[†] Yong-Hong Zhang,[‡] Qin Xu,*[,†] and Dong-Qing Wei*[,†]

[†]State Key Laboratory of Microbial Metabolism and School of Life Sciences and Biotechnology, Shanghai Jiao Tong University, 800 Dongchuan Road, Shanghai 200240, China

[‡]Medicine Engineering Research Center, School of Pharmacy, Chongqing Medical University, Chongqing 400016, China

Supporting Information

ABSTRACT: Alzheimer's disease (AD) is one of the most common dementia. The aggregation and deposition of the amyloid-β peptide (Aβ) in neural tissue is its characteristic symptom. To destabilize and dissolve Aβ fibrils, a number of candidate molecules have been proposed. wgx-50 is a compound extracted from Sichuan pepper (*Zanthoxylum bungeanum*) and a potential candidate drug for treating AD. Our early experiments show it is effective in disassembling Aβ42 aggregations. A series of molecular dynamics simulations were performed in this work to explain the molecular mechanism of the destabilization of Aβ42 protofibril by wgx-50. It is found that there were three possible stable binding sites including two sites in hydrophobic grooves on surface of Aβ protofibril that made no significant changes in Aβ structures and one site in the interior that caused destabilization of the protofibril. In this site, wgx-50 was packed against the side chains of I32 and L34, disrupted the D23−K28 salt bridges, and partially opened the tightly compacted two β-sheets. The results were confirmed by simulations at 320 K, where deeper insertion of wgx-50 into the whole protofibril was observed. The molecular mechanism of this novel drug candidate wgx-50 to disaggregate Aβ protofibril may provide some insight into the strategy of structure-based drug design for AD.

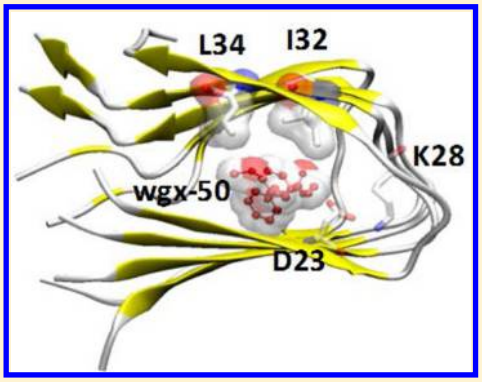

INTRODUCTION

Abnormal aggregates of misfolded proteins are associated with a number of fatal neurodegenerative diseases, including Alzheimer's disease (AD), Huntington's disease (HD), Parkinson's disease (PD), familial British dementia (FED), familial Danish dementia (FDD), and type II diabetes.[1−6] In these diseases, AD is the most common dementia, with rapid increasing incidences and demands for treatments.[7] The physiological mechanism for AD is not fully understood yet; one of the major symptoms of AD is the presence of amyloid plaques in brain, which mainly consist of fibrils of the amyloid-β peptide (Aβ).[8] The "amyloid hypothesis" suggested the aggregation and deposition of the Aβ peptide in neural tissue to be the key of the AD.[9] Although the most toxic species of Aβ is thought to be soluble oligomers,[10,11] a series of studies also suggested possible contribution from insoluble fibrils to the neurotoxicity in various ways.[12−14]

Various candidates targeting on Aβ have been proposed, including antibodies, peptidal inhibitors, and nonpeptidal small molecules. For example, recent in vitro studies have suggested that some polyphenolic compounds from red wine and green tea may bind to Aβ, inhibit Aβ aggregation, and destabilize preformed fibrils.[15,16] In vivo experiments on the Alzheimer's mouse model found a lowered level of amyloid plaque and improved memory and cognitive ability after feeding of red wine.[17,18] Encouraged by these successful results, Riviere et al. proposed a hypothesis that the interactions between resveratrol derivative and Aβ could shift the equilibration of Aβ polymorphism from β-sheets into disordered monomers.[19]

The advances in searching for Aβ fibrils' inhibitors are encouraging; however, the molecular details of the interactions between the inhibitors and the Aβ peptide were often unknown. This situation was gradually changed by progress in investigations of the structures of Aβ fibrils, especially after a 3D structure was determined in 2005.[20] The units of Aβ fibrils are generated by sequential cleavage of β and γ secretases from the amyloid precursor protein (APP) into peptides of 40 or 42 amino acids, indicated by Aβ40 and Aβ42, respectively. Compared with Aβ40, Aβ42 has a stronger tendency to aggregate and comprises the dominant portion of Aβ plaques in AD patients;[21−24] however, both of them may have a common structural motif of strand-loop-strand, which is aligned into two stacked β-sheets and further assembled into cross-β structures in several hypothetical ways.

Special Issue: Biman Bagchi Festschrift

Received: March 31, 2015
Revised: May 15, 2015
Published: May 21, 2015

DOI: 10.1021/acs.jpcb.5b03116
J. Phys. Chem. B 2015, 119, 11196−11202

The understandings in structures of Aβ fibrils boosted the structure-based design of inhibitors targeting on them; however, partially due to the polymorphism of Aβ oligomers or their higher order polymers, many difficulties were encountered in the studies on molecular details of the interactions between Aβ polypeptides and their inhibitors or on possible destabilization mechanisms using traditional experimental methods. On the contrary, computational methods like molecular docking and molecular dynamics simulations exhibited attractive advantages and have been successfully employed in the design of Aβ aggregation inhibitors in recent years. For example, using molecular dynamics simulations, Wu and coworkers characterized the binding sites of a fluorescent dye, Thioflavin T (ThT), and its derivatives on protofibrils of both $A\beta_{9-40}$ and $A\beta_{17-42}$. A common binding motif consists of grooves formed by hydrophobic or aromatic residues on the β-sheet surface along the fibril axis.[25−27] The Klimov group studied anti-inflammatory agents, ibuprofen and naproxen, which may bind to the ends of amyloid fibrils to prevent fibril growth by a competitive mechanism, without significant change in the structure of Aβ peptides.[28−30] Similar studies by Lemkul and Bevan got even more exciting results on morin, an effective antiaggregation flavenoid. It was found that morin not only bound to the ends of $A\beta_{17-42}$ to block further combination of incoming peptides but also intruded into the hydrophobic core to disrupt interior interactions like D23−K28 salt bridges and backbone hydrogen bonds.[31]

In addition to the inhibitors above, *N*-[2-(3,4-dimethoxyphenyl)ethyl]-3-phenyl-acrylamide, or named wgx-50 (earlier as gx-50), was designed by Wei et al.[32] and found in extracts of a natural flavoring vegetation, Sichuan peper (*Zanthoxylum Bungeanum*) (Figure 1). This novel drug

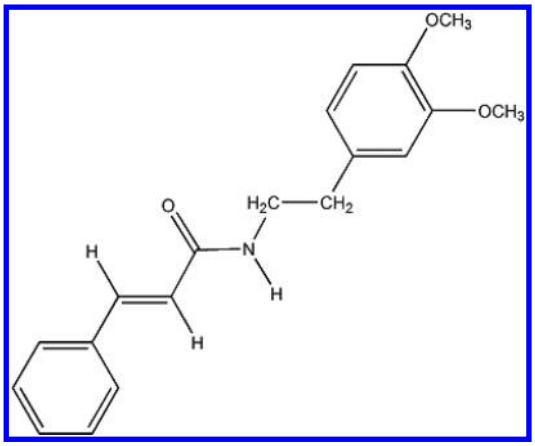

Figure 1. Diagram of a wgx-50 molecule.

candidate was suggested to possibly be an effective therapeutic agent for AD based on a series of biological experiments: in vitro experiments demonstrated that wgx-50 could disassemble Aβ oligomers, inhibit Aβ-induced neuronal apoptosis and apoptotic gene expression, and reduce neuronal calcium toxicity; in vivo experiments showed that wgx-50 could pass the blood brain barrier, decrease the accumulation of Aβ oligomers in the cerebral cortex, and improve the cognitive abilities of mice.[33] Found in natural food products, nontoxic in clinically relevant doses, capable of passing through the blood−brain barrier,[17,18] and effective in Aβ aggregate destabilization in vitro and in vivo, wgx-50 has many advantages to be an attractive therapeutic candidate; however, the molecular mechanism for wgx-50 to destabilize the Aβ42 fibrils is still unclear, which is to be studied in this work using molecular dynamics simulations, so that further structure-based drug design and development could be applied to this type of inhibitors rationally.

METHODS

Models of Aβ42 Protofibrils. The models for simulations were constructed based on the solid-state NMR structure of Aβ protofibril determined by Luhrs et al. (PDB entry 2BEG).[20] Distinct from soluble oligomeric species of Aβ, this pentameric structure is a repeat unit of the mature Aβ fibril and was described as a protofibril or a cross-β subunit.[34] In this structure, each peptide monomer has the disordered N-terminal residues 1−16 missing. The remaining residues 17−42 were suggested to contribute the stability of the mature fibril mostly and were included in the simulation models here. This single cross-β subunit contains five identical peptides of residues 17−42, labeled as A−E (Figure 2), with a strand-loop-strand motif,

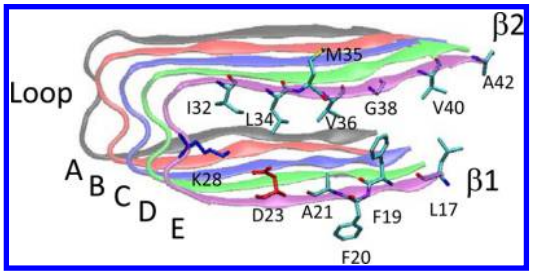

Figure 2. Initial model of $A\beta_{17-42}$ pentamer constructed from the solid-state NMR structure. The five peptide chains A−E are colored in black, red, blue, green, and purple, respectively. The residues important to the stabilization of the fibril are show in sticks. The two residues of the salt bridge, D23 and K28, are colored in red and blue, respectively.

consisting of two in-register stacked β-sheets whose side chains zip against each other in an antiparallel way. In this subunit, the direction of backbone hydrogen bonds paralleled to the fibril axis, with the β-strands perpendicular to it. Each U-shape peptide consists of an N-terminal β-strand (β1) including residues V18−S26, a C-terminal β-strand (β2) including residues I31−A42, and a loop (residues N27−A30) connecting them (Figure 2).

MD Simulation Protocol. All models of $A\beta_{17-42}$ molecule with or without wgx-50 were solvated in a cubic box including about 11 000 water molecules more than 11 Å away from the model border. The solvent water molecules were explicitly represented by the TIP3P model.[35] Five positive sodium ions (Na^+) were added to neutralize the system. Periodic boundary conditions were applied in all directions. Following steepest descent minimizations, each of the systems was equilibrated with positional restraints applied to peptide heavy atoms. With all of the positional restraints released, the models were simulated for 150 ns molecular dynamics (MD) simulations under NPT conditions at 300/320 K and 1 atm. All of the simulations were run using the GROMACS package program[36] with the all-atom AMBER ff03 force field,[37] which shows a good balance between helix and sheet.[25,38] Berendsen's coupling algorithm[39] was applied to keep the temperature and pressure constant, and the LINCS algorithm[40] was used to constrain the lengths of all bonds, so as to extend the

DOI: 10.1021/acs.jpcb.5b03116
J. Phys. Chem. B 2015, 119, 11196−11202

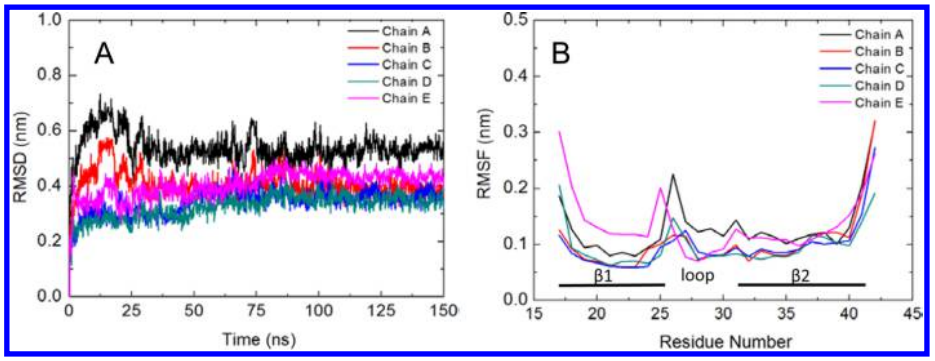

Figure 3. (A) Root-mean-square deviation (RMSD) values and (B) root-mean-square fluctuations (RMSFs) of the five chains during the simulation with Aβ protofibril alone. The colors of the five chains are same to those in Figure 2.

integration time step to 2 fs. The trajectories were saved every 10 ps for the following analyses. The short-range van der Waals (VDW) interactions were treated using a 1.4 nm cutoff, and long-range electrostatic forces were calculated by the Particle Mesh Ewald (PME) method.[41] The parameters of the wgx-50 molecule were from the AMBER GAFF parameter set.[42]

Analysis Details. Binding free energies were calculated using molecular mechanics/generalized Born surface area (MM-GBSA) in the AMBER package.[43] The global structural stability of the pentamer is measured by root-mean-square deviation (RMSD) of the backbone atoms with respect to initial minimized structure, while the root mean-square atomic fluctuation (RMSF) was calculated for Cα atoms of each individual residue. The D23−K28 salt-bridge distances were calculated between the mass centers of the Nζ-amino groups and corresponding Cγ-carboxylates. The average intrachain and interchain distances of β1 and β2 were calculated by the mass center of the residues A21 and V36. The average interchain distances were calculated as the average of distances of the mass centers of all the Cα atoms of neighboring chains. The hydrophobic interactions between wgx-50 and Aβ protofibril were evaluated by the number of hydrophobic contacts, which was defined as any contact between a side chain carbon atom and any carbon atom in wgx-50 within a distance of 0.6 nm. The structures were visualized and figured by the VMD package.[44]

RESULTS AND DISCUSSION

Simulations of Aβ Protofibril Alone at 300 K. Visual inspection of the 150 ns trajectory of the model for Aβ protofibril alone suggested that the overall Aβ structures were quite stable; only small deviations from the initial structure were observed. The major parts of the β-strands were tightly packed to each other without dissociation, and the secondary structures of the strand-loop-strand motif were well-preserved. In the two open end of the β-strands, minor twisting made the five chains not entirely coplanar, optimized side-chain packing, hydrogen bonds, and electrostatic interactions, and somewhat contributed to amyloid fibril stability as proposed previously[45] (Figure S1 in the Supporting Information (SI)).

The overall structural stability of the fibril was measured by RMSD of the backbone atoms with respect to initial model of the minimized crystal structure. The five peptide chains were all generally stable, with the RMSD values as ~0.5 nm, indicating a very low level of overall structural variations (Figure 3A). From the RMSF profile (Figure 3B), it is clear that this stability mainly comes from the two β-strands, where the hydrophobic side chains of F19, A21, I32, L34, V36, and so on packed tightly. The most flexible regions of each peptide were the residues at the N- and C-terminal as well as the residues S26 and I31 connecting the β-strands and the loop. In this model, the terminal residues in the open ends of β-strands were mostly exposed to the solvent and resulted in large fluctuations. Especially on the β1-strands at C-terminal, two residues I41 and A42 beyond the β2-strands at N-terminal are even more exposed and resulted in even higher flexibilities. Another contribution to the overall stability of Aβ protofibril is the stabilization of the loop region by the interchain salt-bridges between residues D23 and K28, similar to many studies that suggested the importance of the D23−K28 salt bridge.[45,46] Most of the D23−K28 salt bridges were maintained during the whole simulations, with the average distances between the Nζ-amino groups and corresponding Cγ-carboxylates being ~0.35 ± 0.05 nm.

Binding of wgx-50 to Aβ Protofibril at 300 K. The same procedure of 150 ns simulations of Aβ alone was repeated four times at 300 K for the model of Aβ fibril with a wgx-50 molecule, in which three possible binding sites were found, shown as sites A, B, and C (Figure 4). Binding sites A and B

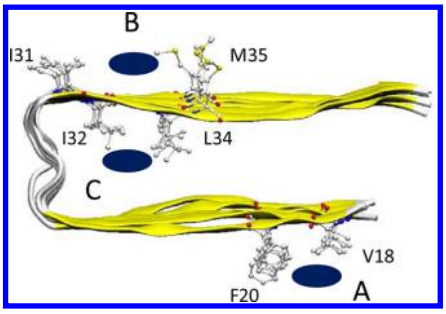

Figure 4. Three binding sites of wgx-50 on Aβ protofibril at 300 K: (A) V18−F20 groove on surface of the β1 sheet layer. (B) I31−M35 groove on surface of the β2 sheet layer. (C) Inserted site in the hydrophobic interior against the I32 and L34 side chains. For clarity, here the Aβ protofibril is simply illustrated by the initial model, and the positions of the three binding sites are indicated by blue ellipses.

reside in the V18−F20 groove on the surface of the β1 sheet layer and the I31−M35 groove on the surface of the β2 sheet layer, respectively (Figure S2 in the SI). These two grooves are between side chains of hydrophobic/aromatic residues, more favorable for the hydrophobic wgx-50 to bind. Previous simulations also suggested that hydrophobic/aromatic and steric interactions are stabilizing forces for binding of several

DOI: 10.1021/acs.jpcb.5b03116
J. Phys. Chem. B 2015, 119, 11196−11202

ligands.[25] Site C is in the interior of the pentameric Aβ fibril, between the side chains of I32 and L34 and the salt bridge between D23 and K28. All three binding sites for wgx-50 were also observed in previous simulations on other Aβ−ligand complexes. Cook predicted the hydrophobic cleft between V18 and F20 as a plausible binding site for $[Ru(bpy)_2dppz]^{2+}$.[47] Both sites on the surface were characterized in the binding of ThT and its derivatives on Aβ fibril.[25] Partial insertion of morin into the hydrophobic core was also founded in Lemkul's simulations.[48]

In the several repeats of 150 ns MD simulations at 300 K and also at an elevated temperature 320 K as discussed later, only binding to the three sites here was observed to be stable enough to keep the ligand from escaping away. On the basis of MM/GBSA calculations, the insertion site has a binding energy of −35.5 kcal/mol, which is much stronger than the −12.3 kcal/mol of site A and −20.5 kcal/mol of site B. They are not guaranteed to be the only possible binding modes, but based on the results we have, we would believe that they are the most possible ones. In the four repeats of simulations at 300 K, one has wgx-50 stably bound at site A, one at site B, and two have it inserted into site C. The higher binding energy and the higher frequency to be observed in limited times of simulations may suggest the higher possibility for wgx-50 to be inserted into site C, and the influence of insertion to site C is also different with binding to site A or B. RMSD profiles suggested that the binding of wgx-50 to the sites A and B on the surface of the Aβ protofibril had little effect on its global stability, while the insertion into site C resulted in significant destabilization. (Figure S3 in the SI). Therefore, it is reasonable to assume two possible roles of wgx-50 in antiaggregation of Aβ fibril: (1) It binds to the two sites on surface to hinder stacking of multilayers of the fibrils into cross-β complexes and hence to ease aggregation; (2) it is inserted into the interior site C, causes significant deformation of the cross-β subunit, and stops assembly of the Aβ fibril.

It is interesting to notice that all three binding sites above were not predicted by a preliminary semiflexible docking using Autodock 4.2. When flexible wgx-50 was docked onto the rigid initial model of Aβ protofibril from the PDB structure 2BEG, the top predicted binding sites were mainly along the edge at chain A of the cross-β subunit, exterior to the binding site C, but in the initial model there is not enough space to accommodate the ligand. Therefore, it is impossible to find site C by docking it onto the rigid initial model. In MD simulations, the ligand was also observed to be temporarily around those sites, but finally it was gradually inserted into site C, with expansion of the interior space and partial deformation of the cross-β subunit as described later. Although the grooves at site A or B were not listed as top binding sites in docking, the binding energies could be enough for them to hold the ligand, in which necessary conformational changes and formation of strong hydrophobic interactions with surrounding residues may help to stabilize the bound state. These dynamic "induced fit" bindings to the three sites require MD simulations to describe the necessary conformational changes in Aβ protofibril and could not be simply predicted by general semiflexible docking procedure using a rigid target. Or in other words, our MD protocol is equivalent to an extensive docking with full flexibility considered for both the ligand and the target.

Destabilization of Aβ Protofibril by wgx-50 Insertion. In all simulations with wgx-50 inserted into the interior of Aβ protofibril, the entry of wgx-50 was always from the edge of chain A, somewhat similar to the binding preference of ibuprofen to the concave (CV) edge simulated by Klimov et al.[30] In one simulation, wgx-50 was rapidly inserted into the hydrophobic interior of the Aβ protofibril within 40 ns, establishing a large number of hydrophobic contacts with side chains inside the two β-sheets of the protofibril. These hydrophobic interactions might be the reason to allow the insertion of wgx-50 into the interior of Aβ protofibrils, similar to the preferred binding to the hydrophobic grooves of sites A and B. The most important hydrophobic interaction is between the aromatic rings of wgx-50 and the side chains of I32 and L34 on chains A−C (Figure 5), which forced the layer of β2 sheet

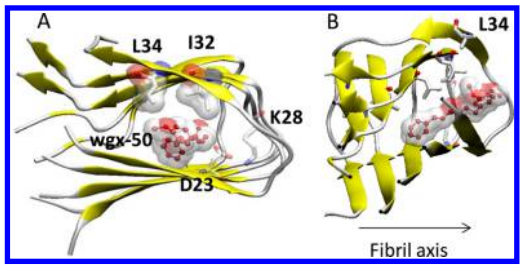

Figure 5. Insertion of wgx-50 into site C at 300 K shown by the final snapshot from top view (A) and alternate view (B). The packing of wgx-50 (in ball and stick) against the side chains of I32 and L34 (in stick) is visualized by surface rendering. The positions of D23 and K28 are also indicated by sticks.

to be contorted, and partially opened the tightly compacted structure of the cross-β subunit. The compactness of the hydrophobic core comprising the β2 portion of the fibril may be a crucial stabilization element in aggregation and elongation of Aβ aggregates.[49,50]

The partial opening of the cross-β-subunit by wgx-50 insertion destabilized the protofibril. The RMSD of the backbone atoms increased to almost 0.75 nm, suggesting an important destabilization of the Aβ protofibril. The RMSFs of the residues were slightly increased, meaning higher flexibilities of the chains after the wgx-50 insertion. This insertion also affected local conformations. The average distances between the charged moieties of the D23−K28 salt bridges were greater than 0.53 nm, far longer than the value of 0.35 nm in simulations of Aβ protofibril alone (Figure 6C). The integrity of the interchain salt bridges has been proposed to be an important contribution in the stability of the Aβ fibril, especially for the loop region.

In addition to corruption of the salt bridges, the number of the backbone hydrogen bonds between chain A and chain B was lowered to around 14 in the simulations after wgx-50 was inserted at site C, well below the control value of 19 hydrogen bonds in the simulations of Aβ protofibril alone (Figure S5 in the SI). The binding energy between chain A and chain B also decreased from −116.2 to −104.5 kcal/mol. The average interchain distances were calculated by the mass centers of all the Cα atoms of each chain. The distance of Aβ protofibril alone is in good agreement with the experimental value as 0.48 ± 0.05 nm of the parallel β-sheets reported by Balbach et al.[51] At the same time, Aβ protofibril with wgx-50 inserted has this distance slightly increased to 0.53 nm, suggesting a tendency of detachment between the peptides. (Figure 6D)

The insertion of wgx-50 into site C caused contortion of the cross-β-subunit and dramatic rearrangement of two strands β1 and β2. With wgx-50 inserted, the two β-strands of the same

DOI: 10.1021/acs.jpcb.5b03116
J. Phys. Chem. B 2015, 119, 11196−11202

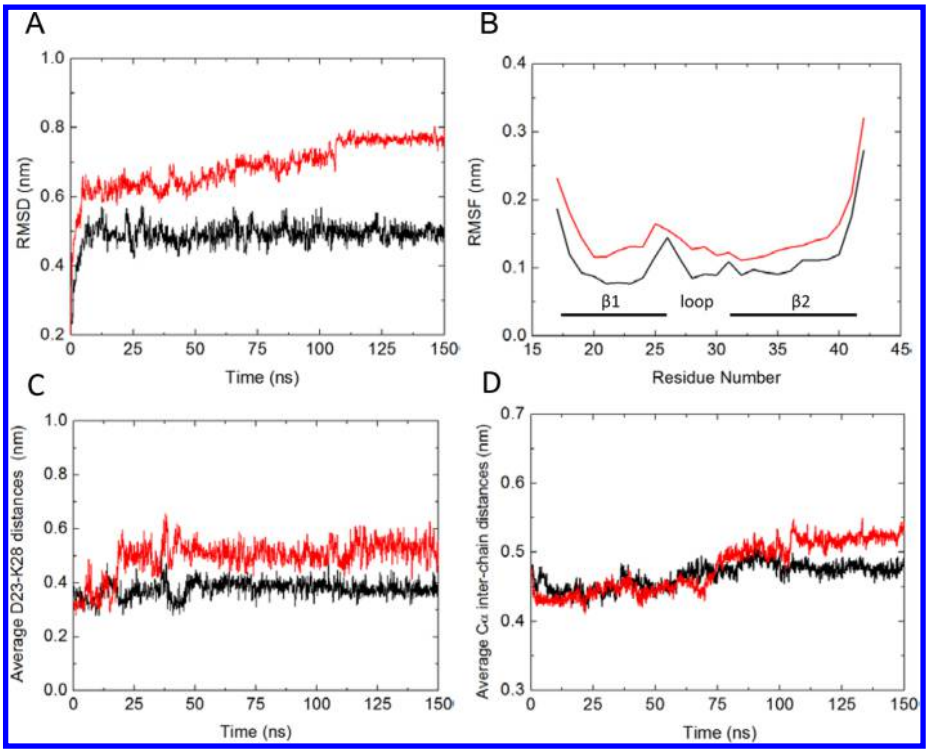

Figure 6. Destabilization of Aβ protofibril by wgx-50 insertion at 300 K. (A) RMSD of the backbone atoms. (B) Root-mean-square fluctuation (RMSF). (C) D23−K28 distances between the mass centers of the Nζ-amino groups and corresponding Cγ-carboxylates. (D) Average interchain distances between the mass centers of all the Cα atoms of neighboring chains are compared between the simulations with Aβ protofibril alone (black) and with wgx-50 inserted in site C (red).

chain significantly moved away from each other, resulting in a small translational shift between the two sheet layers and partial opening of the U-shape structure of the β-strand-loop-β-strand motif, especially at the chains A, B, and C (Figure 5). The loss of hydrophobic contacts between A21 and V36 was observed by calculating the distances between the centers of mass of A21 and V36. All interchain distances between A21 and V36 increased obviously. In particular, between chains A and B and between chains B and C, the distances were increased by 0.42 and 0.70 nm, respectively (Figure 7). Also, the average intrachain A21−V36 distance was increased by 0.31 nm compared with the model of Aβ alone. (Figure S4 in the SI) The variations in the A21−V36 distances are obvious indications of the rearrangement of the parallel, in-register, tightly compacted β-strand-loop-β-strand motifs, which are the basis of a cross-β subunit,[52] and a possible binding intermediate Aβ fibril elongation.[53]

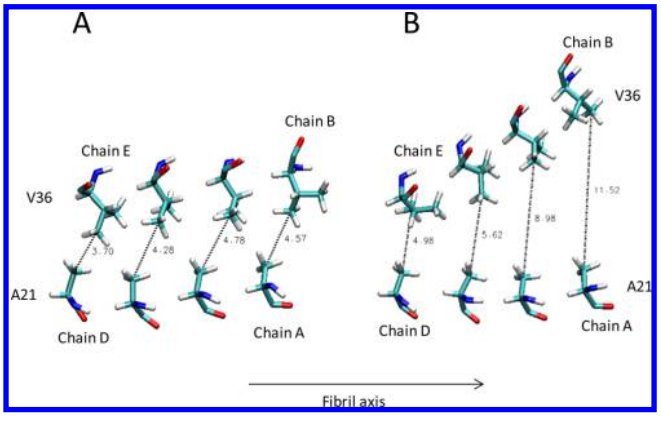

Figure 7. Rearrangement of the β1 and β2 strands indicated by the increased interchain distances of A21 and V36 in the final snapshots of the simulations of Aβ protofibril alone (A) and with wgx-50 inserted at 300 K (B) from the view same to Figure 5B.

Simulations of Aβ Protofibril with wgx-50 at 320 K. The simulations of Aβ protofibril with wgx-50 were repeated at 320 K, slightly elevated from 300 K to compare the influence of stronger hydrophobic interactions. The results were similar to those at 300 K. The only difference was that here wgx-50 penetrated more deeply into the hydrophobic interior of Aβ protofibril and packed against the side chains of I32 and L34 of chains A, B, C, and even D (Figure S6A in the SI). The interchain A21−V36 distances were also increased. Different from the simulation at 300 K, the A21−V36 distances of chains C−D and chains D−E also increased significantly due to the deeper insertion (Figure 8).

As previously suggested, the hydrophobic interactions are possibly the major contributions for the binding of wgx-50 to Aβ protofibril. Thus, the number of hydrophobic contacts between wgx-50 and Aβ protofibril were compared between the insertion simulations at 300 and 320 K. As shown in (Figure S6B in the SI), the number of atomic contacts between the peptides and wgx-50 increased to the maximum sharply within the first 5 ns at 320 K, much faster than in the simulations at 300 K, where it took 45 ns to reach the maximum and became stable. Because the wgx-50 was inserted into the hydrophobic core deeper at 320 K, the total number of hydrophobic contacts was generally 100 higher than in the simulations at 300 K.

CONCLUSIONS

In this work, the binding of wgx-50 onto Aβ protofibril was simulated by molecular dynamics simulations, where destabi-

DOI: 10.1021/acs.jpcb.5b03116
J. Phys. Chem. B 2015, 119, 11196−11202

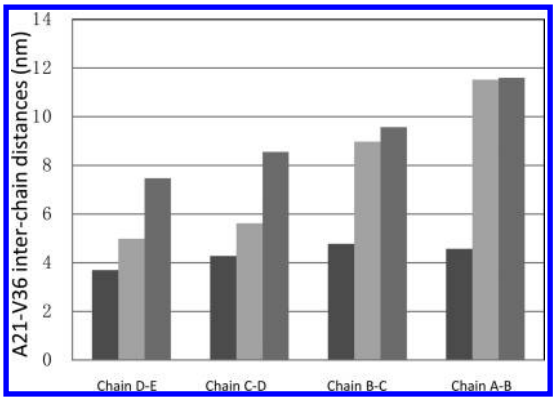

Figure 8. Average A21−V36 interchain distances in simulations of Aβ protofibril alone (dark gray) as well as with wgx-50 inserted at 300 (light gray) and at 320 K (gray).

lization of the protofibril was observed and its molecular mechanism was discussed. Repeats of 150 ns MD simulations found three possible stable binding sites, in which two were in hydrophobic grooves on surface of Aβ protofibril and one was in the interior. Only insertion of wgx-50 into the interior site caused significant destabilization of the protofibril. The aromatic ring of wgx-50 was packed against the side chains of I32 and L34, partially disrupted the D23−K28 salt bridges critical to stabilize the loop region, and extended the distances of A21−V36, which are characteristic of the stacked β-strand-loop-β-strand motifs. The contortion of the parallel β-sheets and the partial opening of the two tightly compacted β-sheets of the cross-β-subunit also destabilized the interactions between the peptides: the number of interchain backbone hydrogen bonds was decreased, the average distances between the peptide chains were enlarged, and the interchain binding energies were lowered. The results were confirmed by simulations repeated at 320 K, where deeper insertion of wgx-50 into the whole protofibril was observed. The molecular dynamics simulations for wgx-50 to destabilize the Aβ protofibril may provide us some insights into the mechanism of this novel drug candidate to disaggregate Aβ fibril and give some hints on the strategy of structure-based drug design for AD.

■ ASSOCIATED CONTENT

Supporting Information

Final snapshot of the simulation of Aβ protofibril alone at 300 K from side view, binding of wgx-50 at site A from the side view of β1 sheet and at site B from the side view of β2 sheet, RMSD of the backbone atoms in all simulations at 300 K, average intrachain A21−V36 distances in the simulations of Aβ alone and with wgx-50 inserted at 300 K, number of the backbone hydrogen bonds between chain A and chain B in the simulations of Aβ alone and with wgx-50 inserted at 300 K, insertion of wgx-50 into the interior of Aβ protofibril at 320 K, and comparison of the numbers of hydrophobic interactions between wgx-50 and the Aβ protofibril during the simulations with wgx-50 inserted at 300 and 320 K. The Supporting Information is available free of charge on the ACS Publications website at DOI: 10.1021/acs.jpcb.5b03116.

■ AUTHOR INFORMATION

Corresponding Authors

*Q.X.: E-mail: xuqin523@sjtu.edu.cn

*D.-Q.W.: E-mail: dqwei@sjtu.edu.cn.

Notes

The authors declare no competing financial interest.

■ ACKNOWLEDGMENTS

D.-Q.W. is supported by grants from the National High-Tech R&D Program (863 Program Contract No. 2012AA020307), the National Basic Research Program of China (973 Program) (Contract No. 2012CB721000), the Key Project of Shanghai Science and Technology Commission (Contract No. 11JC1406400), and Ph.D. Programs Foundation of Ministry of Education of China (Contract No., 20120073110057). Q.X. is supported by grants from National Natural Science Foundation of China for Young Scholars (Grant No. 31400704).

■ REFERENCES

(1) Temussi, P. A.; Masino, L.; Pastore, A. From Alzheimer to Huntington: Why is a Structural Understanding So Difficult? *EMBO J.* **2003**, *22* (3), 355−361.

(2) Cohen, F. E.; Kelly, J. W. Therapeutic Approaches to Protein-Misfolding Diseases. *Nature* **2003**, *426* (6968), 905−909.

(3) Dobson, C. M. Protein Folding and Misfolding. *Nature* **2003**, *426* (6968), 884−890.

(4) Chiti, F.; Dobson, C. M. Protein Misfolding, Functional Amyloid, and Human Disease. *Annu. Rev. Biochem.* **2006**, *75*, 333−66.

(5) DeToma, A. S.; Salamekh, S.; Ramamoorthy, A.; Lim, M. H. Misfolded Proteins in Alzheimer's Disease and Type II Diabetes. *Chem. Soc. Rev.* **2012**, *41* (2), 608−621.

(6) Eisenberg, D.; Jucker, M. The Amyloid State of Proteins in Human Diseases. *Cell* **2012**, *148* (6), 1188−1203.

(7) Goedert, M.; Spillantini, M. G. A Century of Alzheimer's Disease. *Science* **2006**, *314* (5800), 777−781.

(8) Monsonego, A.; Zota, V.; Karni, A.; Krieger, J. I.; Bar-Or, A.; Bitan, G.; Budson, A. E.; Sperling, R.; Selkoe, D. J.; Weiner, H. L. Increased T Cell Reactivity to Amyloid Beta Protein in Older Humans and Patients with Alzheimer Disease. *J. Clin. Invest.* **2003**, *112* (3), 415−422.

(9) Hardy, J. A.; Higgins, G. A. Alzheimer's Disease: the Amyloid Cascade Hypothesis. *Science* **1992**, *256* (5054), 184−185.

(10) Kayed, R.; Head, E.; Thompson, J. L.; McIntire, T. M.; Milton, S. C.; Cotman, C. W.; Glabe, C. G. Common Structure of Soluble Amyloid Oligomers Implies Common Mechanism of Pathogenesis. *Science* **2003**, *300* (5618), 486−489.

(11) Lesne, S.; Koh, M. T.; Kotilinek, L.; Kayed, R.; Glabe, C. G.; Yang, A.; Gallagher, M.; Ashe, K. H. A Specific Amyloid-Beta Protein Assembly in the Brain Impairs Memory. *Nature* **2006**, *440* (7082), 352−357.

(12) Tsai, J.; Grutzendler, J.; Duff, K.; Gan, W. B. Fibrillar Amyloid Deposition Leads to Local Synaptic Abnormalities and Breakage of Neuronal Branches. *Nat. Neurosci.* **2004**, *7* (11), 1181−1183.

(13) Deshpande, A.; Mina, E.; Glabe, C.; Busciglio, J. Different Conformations of Amyloid Beta Induce Neurotoxicity by Distinct Mechanisms in Human Cortical Neurons. *J. Neurosci.* **2006**, *26* (22), 6011−6018.

(14) Picone, P.; Carrotta, R.; Montana, G.; Nobile, M. R.; San Biagio, P. L.; Di Carlo, M. Abeta Oligomers and Fibrillar Aggregates Induce Different Apoptotic Pathways in LAN5 Neuroblastoma Cell Cultures. *Biophys. J.* **2009**, *96* (10), 4200−4211.

(15) Ono, K.; Yoshiike, Y.; Takashima, A.; Hasegawa, K.; Naiki, H.; Yamada, M. Potent Anti-Amyloidogenic and Fibril-Destabilizing Effects of Polyphenols in Vitro: Implications for the Prevention and Therapeutics of Alzheimer's Disease. *J. Neurochem.* **2003**, *87* (1), 172−181.

(16) Hamaguchi, T.; Ono, K.; Yamada, M. Anti-Amyloidogenic Therapies: Strategies for Prevention and Treatment of Alzheimer's Disease. *Cell. Mol. Life Sci.* **2006**, *63* (13), 1538−1552.

DOI: 10.1021/acs.jpcb.5b03116
J. Phys. Chem. B 2015, 119, 11196−11202

(17) Ho, L.; Chen, L. H.; Wang, J.; Zhao, W.; Talcott, S. T.; Ono, K.; Teplow, D.; Humala, N.; Cheng, A.; Percival, S. S.; et al. Heterogeneity in Red Wine Polyphenolic Contents Differentially Influences Alzheimer's Disease-Type Neuropathology and Cognitive Deterioration. *J. Alzheimer's Dis.* **2009**, *16* (1), 59−72.
(18) Wang, J.; Ho, L.; Zhao, W.; Ono, K.; Rosensweig, C.; Chen, L.; Humala, N.; Teplow, D. B.; Pasinetti, G. M. Grape-Derived Polyphenolics Prevent Abeta Oligomerization and Attenuate Cognitive Deterioration in a Mouse Model of Alzheimer's Disease. *J. Neurosci.* **2008**, *28* (25), 6388−6392.
(19) Riviere, C.; Delaunay, J. C.; Immel, F.; Cullin, C.; Monti, J. P. The Polyphenol Piceid Destabilizes Preformed Amyloid Fibrils and Oligomers in Vitro: Hypothesis on Possible Molecular Mechanisms. *Neurochem. Res.* **2009**, *34* (6), 1120−1128.
(20) Luhrs, T.; Ritter, C.; Adrian, M.; Riek-Loher, D.; Bohrmann, B.; Doeli, H.; Schubert, D.; Riek, R. 3D Structure of Alzheimer's Amyloid-Beta(1−42) Fibrils. *Proc. Natl. Acad. Sci. U.S.A.* **2005**, *102* (48), 17342−17347.
(21) Haass, C.; Selkoe, D. J. Soluble Protein Oligomers in Neurodegeneration: Lessons from the Alzheimer's Amyloid Beta-Peptide. *Nat. Rev. Mol. Cell Biol.*. **2007**, *8* (2), 101−112.
(22) Mucke, L.; Masliah, E.; Yu, G. Q.; Mallory, M.; Rockenstein, E. M.; Tatsuno, G.; Hu, K.; Kholodenko, D.; Johnson-Wood, K.; McConlogue, L. High-Level Neuronal Expression of A Beta(1−42) in Wild-Type Human Amyloid Protein Precursor Transgenic Mice: Synaptotoxicity without Plaque Formation. *J. Neurosci.* **2000**, *20* (11), 4050−4058.
(23) Jarrett, J. T.; Lansbury, P. T., Jr. Seeding "One-Dimensional Crystallization" of Amyloid: A Pathogenic Mechanism in Alzheimer's Disease and Scrapie? *Cell* **1993**, *73* (6), 1055−1058.
(24) Selkoe, D. J. Translating Cell Biology into Therapeutic Advances in Alzheimer's Disease. *Nature* **1999**, *399* (6738), A23−A31.
(25) Wu, C.; Bowers, M. T.; Shea, J.-E. On the Origin of the Stronger Binding of PIB over Thioflavin T to Protofibrils of the Alzheimer Amyloid-Beta Peptide: A Molecular Dynamics Study. *Biophys. J.* **2011**, *100* (5), 1316−1324.
(26) Wu, C.; Scott, J.; Shea, J.-E. Binding of Congo Red to Amyloid Protofibrils of the Alzheimer A beta(9−40) Peptide Probed by Molecular Dynamics Simulations. *Biophys. J.* **2012**, *103* (3), 550−557.
(27) Wu, C.; Wang, Z.; Lei, H.; Duan, Y.; Bowers, M. T.; Shea, J.-E. The Binding of Thioflavin T and Its Neutral Analog BTA-1 to Protofibrils of the Alzheimer's Disease A beta(16−22) Peptide Probed by Molecular Dynamics Simulations. *J. Mol. Biol.* **2008**, *384* (3), 718−729.
(28) Raman, E. P.; Takeda, T.; Klimov, D. K. Molecular dynamics simulations of Ibuprofen binding to Abeta peptides. *Biophys. J.* **2009**, *97* (7), 2070−9.
(29) Takeda, T.; Kumar, R.; Raman, E. P.; Klimov, D. K. Nonsteroidal Anti-Inflammatory Drug Naproxen Destabilizes Abeta Amyloid Fibrils: A Molecular Dynamics Investigation. *J. Phys. Chem.B* **2010**, *114* (46), 15394−402.
(30) Chang, W. E.; Takeda, T.; Raman, E. P.; Klimov, D. K. Molecular Dynamics Simulations of Anti-Aggregation Effect of Ibuprofen. *Biophys. J.* **2010**, *98* (11), 2662−2670.
(31) Lemkul, J. A.; Bevan, D. R. Destabilizing Alzheimer's Abeta(42) Protofibrils with Morin: Mechanistic Insights from Molecular Dynamics Simulations. *Biochemistry* **2010**, *49* (18), 3935−3946.
(32) Gu, R. X.; Gu, H.; Xie, Z. Y.; Wang, J. F.; Arias, H. R.; Wei, D. Q.; Chou, K. C. Possible Drug Candidates for Alzheimer's Disease Deduced from Studying Their Binding Interactions with Alpha7 Nicotinic Acetylcholine Receptor. *Med. Chem.* **2009**, *5* (3), 250−262.
(33) Tang, M.; Wang, Z.; Zhou, Y.; Xu, W.; Li, S.; Wang, L.; Wei, D.; Qiao, Z. A Novel Drug Candidate for Alzheimer's Disease Treatment: Gx-50 Derived from Zanthoxylum Bungeanum. *J. Alzheimer's Dis.* **2013**, *34* (1), 203−213.
(34) Shea, J. E.; Urbanc, B. Insights into A beta Aggregation: A Molecular Dynamics Perspective. *Curr. Top. Med. Chem.* **2012**, *12* (22), 2596−2610.
(35) Jorgensen, W. L.; Chandrasekhar, J.; Madura, J. D.; Impey, R. W.; Klein, M. L. Comparison of Simple Potential Functions for Simulating Liquid Water. *J. Chem. Phys.* **1983**, *79* (2), 926−935.
(36) Van der Spoel, D.; Lindahl, E.; Hess, B.; Groenhof, G.; Mark, A. E.; Berendsen, H. J. C. GROMACS: Fast, Flexible, and Free. *J. Comput. Chem.* **2005**, *26* (16), 1701−1718.
(37) Duan, Y.; Wu, C.; Chowdhury, S.; Lee, M. C.; Xiong, G. M.; Zhang, W.; Yang, R.; Cieplak, P.; Luo, R.; Lee, T.; et al. A Point-Charge Force Field for Molecular Mechanics Simulations of Proteins Based on Condensed-Phase Quantum Mechanical Calculations. *J. Comput. Chem.* **2003**, *24* (16), 1999−2012.
(38) Hornak, V.; Abel, R.; Okur, A.; Strockbine, B.; Roitberg, A.; Simmerling, C. Comparison of Multiple Amber Force Fields and Development of Improved Protein Backbone Parameters. *Proteins* **2006**, *65* (3), 712−725.
(39) Berendsen, H. J. C.; Postma, J. P. M.; van Gunsteren, W. F.; DiNola, A.; Haak, J. R. Molecular Dynamics with Coupling to an External Bath. *J. Chem. Phys.* **1984**, *81* (8), 3684−3690.
(40) Hess, B.; Bekker, H.; Berendsen, H. J. C.; Fraaije, J. LINCS: A Linear Constraint Solver for Molecular Simulations. *J. Comput. Chem.* **1997**, *18* (12), 1463−1472.
(41) Darden, T.; York, D.; Pedersen, L. Particle Mesh Ewald: an N.log(N) Method for Ewald Sums in Large Systems. *J. Chem. Phys.* **1993**, *98* (12), 10089−10092.
(42) Wang, J. M.; Wolf, R. M.; Caldwell, J. W.; Kollman, P. A.; Case, D. A. Development and Testing of a General Amber Force Field. *J. Comput. Chem.* **2004**, *25* (9), 1157−1174.
(43) Kollman, P. A.; Massova, I.; Reyes, C.; Kuhn, B.; Huo, S.; Chong, L.; Lee, M.; Lee, T.; Duan, Y.; W, W.; et al. Calculating Structures and Free Energies of Complex Molecules: Combining Molecular Mechanics and Continuum Models. *Acc. Chem. Res.* **2000**, *33*, 889−897.
(44) Humphrey, W.; Dalke, A.; Schulten, K. VMD: Visual Molecular Dynamics. *J. Mol. Graphics Modell.* **1996**, *14* (1), 33−38.
(45) Zheng, J.; Jang, H.; Ma, B.; Tsai, C.-J.; Nussinov, R. Modeling the Alzheimer A Beta(17−42) Fibril Architecture: Tight Intermolecular Sheet-Sheet Association and Intramolecular Hydrated Cavities. *Biophys. J.* **2007**, *93* (9), 3046−3057.
(46) Thirumalai, D.; Klimov, D. K.; Dima, R. I. Emerging Ideas on the Molecular Basis of Protein and Peptide Aggregation. *Curr. Opin. Struct. Biol.* **2003**, *13* (2), 146−159.
(47) Cook, N. P.; Ozbil, M.; Katsampes, C.; Prabhakar, R.; Marti, A. A. Unraveling the Photoluminescence Response of Light-Switching Ruthenium(II) Complexes Bound to Amyloid-Beta. *J. Am. Chem. Soc.* **2013**, *135* (29), 10810−10816.
(48) Autiero, I.; Saviano, M.; Langella, E. In Silico Investigation and Targeting of Amyloid Beta Oligomers of Different Size. *Mol. Biosyst.* **2013**, *9* (8), 2118−2124.
(49) Masman, M. F.; Eisel, U. L.; Csizmadia, I. G.; Penke, B.; Enriz, R. D.; Marrink, S. J.; Luiten, P. G. In Silico Study of Full-Length Amyloid Beta 1−42 Tri- and Penta-Oligomers in Solution. *J. Phys. Chem. B* **2009**, *113* (34), 11710−11719.
(50) Buchete, N.-V.; Hummer, G. Structure and Dynamics of Parallel Beta-Sheets, Hydrophobic Core, and Loops in Alzheimer's A Beta Fibrils. *Biophys. J.* **2007**, *92* (9), 3032−3039.
(51) Balbach, J. J.; Petkova, A. T.; Oyler, N. A.; Antzutkin, O. N.; Gordon, D. J.; Meredith, S. C.; Tycko, R. Supramolecular Structure in Full-Length Alzheimer's Beta-Amyloid Fibrils: Evidence for a Parallel Beta-Sheet Organization from Solid-State Nuclear Magnetic Resonance. *Biophys. J.* **2002**, *83* (2), 1205−1216.
(52) Kirschner, D. A.; Abraham, C.; Selkoe, D. J. X-Ray-Diffraction from Intraneuronal Paired Helical Filaments and Extraneuronal Amyloid Fibers in Alzheimer-Disease Indicates Cross-Beta Conformation. *Proc. Natl. Acad. Sci. U.S.A.* **1986**, *83* (2), 503−507.
(53) Han, W.; Wu, Y. D. A Strand-Loop-Strand Structure is a Possible Intermediate in Fibril Elongation: Long Time Simulations of Amylold-Beta Peptide (10−35). *J. Am. Chem. Soc.* **2005**, *127* (44), 15408−15416.

DOI: 10.1021/acs.jpcb.5b03116
J. Phys. Chem. B 2015, 119, 11196−11202